Surface effects on the elastic modulus of Te nanowires

G. Stan,[1,a] S. Krylyuk,[2] A. V. Davydov,[2] M. Vaudin,[1] L. A. Bendersky,[2] and R. F. Cook[1]
[1]*Ceramics Division, National Institute of Standards and Technology, Gaithersburg, Maryland 20899, USA*
[2]*Metallurgy Division, National Institute of Standards and Technology, Gaithersburg, Maryland 20899, USA*

(Received 7 April 2008; accepted 23 May 2008; published online 17 June 2008)

Nondestructive elastic property measurements have been performed on Te nanowires with diameters in the range 20–150 nm. By using contact resonance atomic force microscopy, the elastic indentation modulus perpendicular to the prismatic facets of the nanowires has been accurately quantified. In this diameter range, a pronounced size dependence of the modulus has been observed: an invariant value consistent with Te bulk properties for large wire diameters, followed by a nonlinear increase with decreasing diameter, and finally an almost doubling of the modulus for Te nanowires thinner than 30 nm. A model based on surface stiffening describes the observations. © *2008 American Institute of Physics*. [DOI: 10.1063/1.2945285]

The ability to investigate the properties of nanostructures enables both the elucidation of physics governing materials at this scale as well as building new functional devices of smaller size. Great effort has been extended recently to fabricate one-dimensional (1D) structures such as nanotubes, nanowires (NWs), and nanobelts[1,2] and to understand their properties as a function of material, size, and shape.[3–7] The unique combination of piezoelectric thermoelectric, and nonlinear optical properties[8] of elemental tellurium (Te), as well as its inherent crystallographic anisotropy, make 1D Te nanostructures very promising candidates for nanoscale electronic and optoelectronic devices.[1] As is the case with any 1D nanostructure, accurate knowledge of the mechanical properties of those made of Te is required prior to integration into functional devices.

In the past few years, various techniques have been developed to provide direct measurements of the mechanical properties of wirelike 1D structures: bending of suspended or as-grown nanofilaments by atomic force microscopy (AFM),[9] static and dynamic nanoindentations,[5,10] transmission electron microscopy (TEM) using *in situ* electromechanical resonance,[11] as well as monitoring the cantilever dynamics in contact resonance AFM (CR-AFM).[6] In this work, the elastic moduli of Te NWs, of various thicknesses in the 20–150 nm range, have been measured using CR-AFM. The indentation modulus on the prismatic facets of the NWs was found to depend on the thickness of the NWs. By considering a surface stiffness enhancement in the outerlayers of NWs as a function of NW thickness, the measured size dependence of the elastic modulus of Te NWs is well explained over the investigated range.

Te nanostructures were grown on Si(100) substrates by a thermal vapor-transport deposition method. At 180 °C, the deposition mainly provided long (2–10 μm) Te NWs of uniform cross section. The morphology of the Te NWs so obtained was examined using a field emission scanning electron microscope (FESEM) (Hitachi S-4700-II) equipped with an electron backscatter diffraction (EBSD) detector.[12] EBSD patterns on the top facets of NWs showed that these facets were crystallographically the same $(10\bar{1}0)$ plane of the Te hexagonal lattice and the NW growth direction was the *c*-axis. Also, single-crystal structure, [0001] growth direction, and faceting of Te NWs were revealed in high-resolution transmission electron microscopy. In Fig. 1 are shown such NWs at different magnifications: A FESEM image in Fig. 1(a) encompasses many Te 1D filaments; a higher magnification AFM image of a Te *T*-junction made by a nanobelt and a nanowire is shown in Fig. 1(b); and in Fig. 1(c) a 500 nm segment of the wire length from Fig. 1(b) is further detailed by AFM scanning. The wire cross section as observed by AFM shown in Fig. 1(c) is rectangular, and this was the case for all the Te NWs investigated here. As the vertical profile of the walls is not resolved accurately by AFM, the observed rectangular cross section could, in fact, originate from an elongated hexagonal section.

In CR-AFM, the contact between an AFM probe and the tested material, in our case the top facet of a NW, is vibrated by a very small amplitude oscillation at frequencies in the kilohertz to megahertz range.[13,14] Here, a lock-in amplifier with an internal signal generator (7280 Signal Recovery AMETEK)[12] was used to mechanically vibrate the AFM cantilever probe forming one-half of the contact and collect the high-frequency response signal from the AFM photodiode detector.[15] This additional instrumentation was connected to

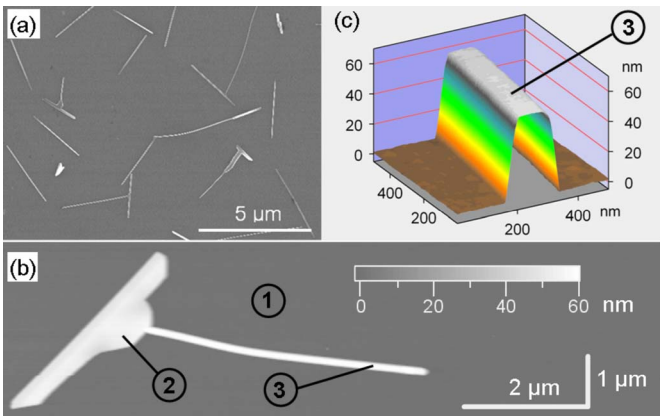

FIG. 1. (Color online) (a) FESEM image of Te NWs. (b) CR-AFM measurements are performed at locations 1, 2, and 3, to measure the contact stiffness on Si(100) substrate, Te nanobelt, and Te NW, respectively. (c) A 500 nm segment of the investigated Te NW is shown in detail using AFM.

[a]Electronic mail: gheorghe.stan@nist.gov.

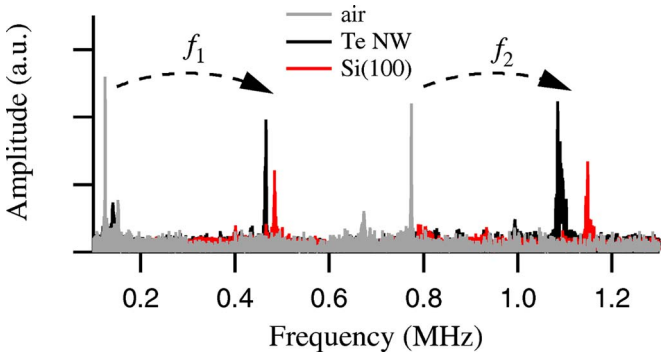

FIG. 2. (Color online) The shift in the resonance frequency of the first two vibrational CR-AFM modes from air to contact on a 25 nm diameter Te NW and Si(100).

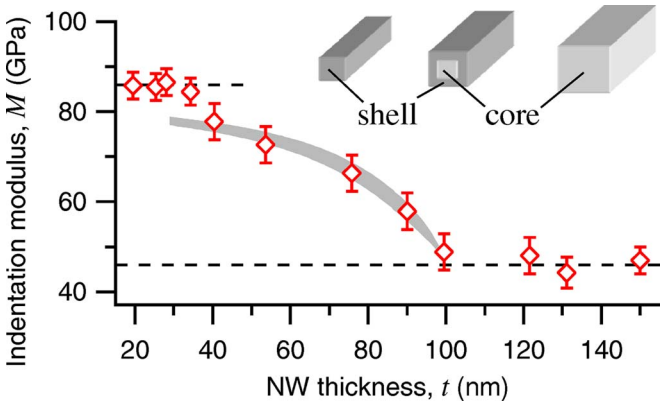

FIG. 3. (Color online) (a) Indentation modulus M of Te NWs as a function of NW thickness. The dashed lines indicate the maximum (very thin NWs) and minimum (very thick NWs) extreme values.

an AFM (Veeco Multimode III).[12] The AFM probes (PPP-SEIH NanoSensors)[12] were single-crystal Si cantilevers made with integrated Si tips. The spring constant k_c of the cantilevers used was around 10 N m^{-1}, as determined by the thermal-noise method.[16] Throughout the measurements, a static load of about 250 nN was constantly maintained on the tip-NW contacts. This applied load was larger than the adhesive contact forces but small enough to produce only elastic deformation at the contact and no deformation contribution from the Si substrate.

When an AFM probe is brought into contact, the resonance frequency of the attached cantilever undergoes an increase determined by the stiffness of the contact between the probe and the sample. This "contact stiffness," $k^\star$, is calculated from the measured resonance frequency by modeling the system as a clamped-coupled vibrating beam.[13,14] In the limit of Hertzian contact mechanics, $k^\star$ is determined by the contact radius, a, and the reduced elastic modulus of the contact, $E^\star$, $k^\star = 2aE^\star$.[17] The reduced elastic modulus is given by the indentation moduli of the tested material, M, and the AFM tip, M_T, $E^\star = (1/M + 1/M_T)^{-1}$. For an isotropic material, the indentation modulus is simply expressed in terms of Young's modulus E and Poisson's ratio ν, $M = E/(1-\nu^2)$, whereas numerical calculation is required for anisotropic materials.[18] In CR-AFM, an accurate quantification of the indentation modulus M of a given material is then provided by the ratio of the contact stiffnesses, $k^\star_{\text{ref}}$ and $k^\star$, obtained from the CR-AFM frequencies measured successively on a reference material of known elastic modulus and the material tested as follows:[19]

$$1/M = (k^\star_{\text{ref}}/k^\star)^{3/2}(1/M_{\text{ref}} + 1/M_T) - 1/M_T. \quad (1)$$

Te NWs of different diameters lying on the same substrate were localized by tapping-mode AFM followed by CR-AFM measurements performed back and forth on top of the wire and the Si(100) substrate, as indicated in Fig. 1(b). Figure 2 shows the shift in the resonance frequency of the AFM cantilever from air to contact on a 25 nm thick Te NW and Si(100) substrate, respectively. The normalized contact stiffness, $k^\star/k_c$, was calculated from the first two contact resonance frequencies by using the clamped-coupled beam model.[13] The corresponding indentation modulus was then calculated by means of Eq. (1). In addition to the contact stiffness values, $M_{\text{Si}(100)} = 164.8$ GPa was used in Eq. (1) for the indentation modulus of the reference substrate and the probe tip.

As the thickness of the NWs decreased, the measured contact resonance frequencies were observed to shift to greater and greater values. In terms of the elastic response, this indicates an increase in the elastic modulus, as can be seen in Fig. 3. Starting from values slightly greater than 45 GPa for NWs thicker than 100 nm, the increasing trend in the indentation modulus plateaued around 85 GPa for NWs with diameters less than 30 nm. A similar enhancement factor of 1.5–2 has been measured, by different techniques, for the size-dependent elastic modulus of other metallic (Ag and Pb)[3] as well as nonmetallic [ZnO (Refs. 4 and 6) and CuO (Ref. 7)] NWs. However, the behavior observed here differs from that reported for other types of NWs for which the elastic modulus was found to increase continuously with the reduction in diameter.[3,4,6,7]

The observed size dependence in the mechanical properties of these nanostructures can be understood by considering a surface stiffness effect[3,4,6] and the large surface-to-volume ratio at the nanoscale.[20] It has been shown in atomistic computer simulations[21] that a significant tensile strain accumulates in the near-surface layers of NWs as a result of the reduced atom coordination and distorted symmetry. This determines, in turn, a progressive lattice contraction from outside to inside and places the inner core in compression. The accumulated strain leads thus to nonlinear elastic effects such that the surface is stiffened relative to the bulk.

To quantify the contribution of surface stiffening to the observed axial Young's modulus of ZnO NWs, Chen *et al.*[4] considered a NW composed of a NW core made of bulk material and a stiffer NW shell of constant thickness, coaxial with the core. Following this interpretation, a linear variation of the shell thickness s as a function of the NW thickness t can be assumed over the elastic modulus size-dependent range in our measurements as follows:

$$2s = t_{\min}(t_{\max} - t)/(t_{\max} - t_{\min}), \quad (2)$$

where $t_{\max}$ and $t_{\min}$ approximately delimitate the size-dependent elastic modulus range: $t_{\max}$ is the NW thickness above which the shell is of negligible thickness and $t_{\min}$ is the NW thickness below which the measured elastic modulus is that of the stiffened shell; core-shell diagrams for the considered thickness range are shown in the inset of Fig. 3. We used a model considering a probe tip indenting the composite shell-core structure, similar to the case of an indented coated

substrate,[22] to separate the elastic contributions of the core and shell in our measurements as follows:

$$M = I(\xi)M_{\text{shell}} + [1 - I(\xi)]M_{\text{core}}. \quad (3)$$

M_{core} and M_{shell} are the indentation moduli of the core and the shell, respectively, and $\xi = s/a$ is the shell thickness s normalized to the contact radius a. $I(\xi) = (2/\pi)\arctan(\xi) + [(1-2\nu)\xi \ln(1+\xi^{-2}) - \xi/(1+\xi^2)]/2\pi(1-\nu)$ is a weighting function of ξ and Poisson's ratio ν, here taken to be the same for both core and shell.

We have applied the above model to fit the measured indentation modulus on Te NWs in the thickness range where the shell is presumably thinner than the core. From the observed plateaus, we deduced a value of approximately 85 GPa for M_{shell} and 46 GPa for M_{core}. With M_{shell} and M_{core} determined from the two limiting regions, a good fit is provided by Eq. (3) in the transition region with fit parameters of $t_{\text{min}} = 29$ nm, $t_{\text{max}} = 100$ nm, and $a = 4$ nm.[23] The fit given by the model is within the gray band in Fig. 3 as the Poisson's ratio was varied from 0.1 (upper edge) to 0.4 (lower edge). The applicability of the model is restricted from the domain of thin NWs in which the core is reduced in thickness so much that it cannot be considered as a substrate for the indented shell. Very little variation in the elastic modulus is observed for NWs thinner than 30 nm, suggesting that when the shell extends over the entire NW thickness, the attendant lattice contraction and disorder is less of an energy penalty than that required to reach the equilibrium interatomic order of the bulk core. The average thickness of the shell for the Te NWs measured here, $t_{\text{min}}/4 = 7.2$ nm, is comparable with the values reported previously for ZnO NWs, 4.4 (Ref. 4) and 12 nm,[6] respectively. Here, a caveat regarding overinterpretation is in order: A different shell thickness is implied by the 12% reduction in indentation modulus observed in our measurements for a wide nanobelt compared with a NW of the same thickness [locations 2 and 3 in Fig. 1(b)]. This observation, consistent with the recently measured width-to-thickness dependence of the elastic modulus of ZnO nanobelts,[5] suggests an aspect-ratio dependence for moduli, as well as a scale dependence for nanostructures.

Although the above interpretation is more intuitive than fundamental, it captures the size-dependent effects observed in elastic modulus measurements on NWs and provides a simple explanation for the surface stiffness enhancement in NWs of reduced diameters that must limit more physically based explanations drawn from atomistic modeling[21] or first-principles density functional theory.[24]

[1] Y. Xia, P. Yang, Y. Sun, Y. Wu, B. Mayers, B. Gates, Y. Yin, F. Kim, and H. Yan, Adv. Mater. (Weinheim, Ger.) **15**, 353 (2003).
[2] Z. L. Wang, J. Phys.: Condens. Matter **16**, R829 (2004).
[3] S. Cuenot, C. Fretigny, S. Demoustier-Champagne, and B. Nysten, Phys. Rev. B **69**, 165410 (2004).
[4] C. Q. Chen, Y. Shi, Y. S. Zhang, J. Zhu, and Y. J. Yan, Phys. Rev. Lett. **96**, 075505 (2006).
[5] M. Lucas, W. Mai, R. Yang, Z. L. Wang, and E. Riedo, Nano Lett. **7**, 1314 (2007).
[6] G. Stan, C. V. Ciobanu, P. M. Parthangal, and R. F. Cook, Nano Lett. **7**, 3691 (2007).
[7] E. P. S. Tan, Y. Zhu, T. Yu, L. Dai, C. H. Sow, V. B. C. Tan, and C. T. Lim, Appl. Phys. Lett. **90**, 163112 (2007).
[8] A. A. Kudryavstev, *The Chemistry and Technology of Selenium and Tellurium*, (Collet's Ltd., London, 1974).
[9] J.-P. Salvetat, A. J. Kulik, J.-M. Bonard, G. A. D. Briggs, T. Stöckli, K. Motonier, S. Bonnamy, F. Boguin, N. A. Burnham, and L. Forro, Adv. Mater. (Weinheim, Ger.) **11**, 161 (1999); J. H. Song, X. D. Wang, E. Riedo, and Z. L. Wang, Nano Lett. **5**, 1954 (2005).
[10] X. Li, H. Gao, C. J. Murphy, and K. K. Caswell, Nano Lett. **3**, 1495 (2003).
[11] P. Poncharal, Z. L. Wang, D. Ugarte, and W. A. de Heer, Science **283**, 1513 (1999).
[12] Any mention of commercial products in this paper is for information only; it does not imply recommendation or endorsement by NIST.
[13] U. Rabe, K. Janser, and W. Arnold, Rev. Sci. Instrum. **67**, 3281 (1996).
[14] K. Yamanaka and S. Nakano, Jpn. J. Appl. Phys., Part 1 **35**, 3787 (1996).
[15] G. Stan and W. Price, Rev. Sci. Instrum. **77**, 103707 (2006).
[16] J. L. Hutter and J. Bechhoefer, Rev. Sci. Instrum. **64**, 1868 (1993).
[17] K. L. Johnson, *Contact Mechanics* (Cambridge University Press, Cambridge, 1996).
[18] J. J. Vlassak and W. D. Nix, Philos. Mag. A **67**, 1045 (1993).
[19] U. Rabe, S. Amelio, M. Kopycinska, S. Hirsekorn, M. Kempf, M. Goken, and W. Arnold, Surf. Interface Anal. **33**, 65 (2002).
[20] C. Q. Sun, B. K. Tay, X. T. Zeng, S. Li, T. P. Chen, J. Zhou, H. L. Bai, and E. Y. Jiang, J. Phys.: Condens. Matter **14**, 7781 (2002).
[21] A. J. Kulkarni, M. Zhou, and F. J. Ke, Nanotechnology **16**, 2749 (2005); Y. Wen, Y. Zhang, and Z. Zhu, Phys. Rev. B **76**, 125423 (2007).
[22] H. Gao, C.-H. Chiu, and J. Lee, Int. J. Solids Struct. **29**, 2471 (1992).
[23] The fit parameter $a = 4.0$ nm aggrees well with the contact radius, $a = 4.2$ nm, calculated with the Hertz model, $a = (3PR/4E^*)^{1/3}$, for a load $P = 250$ nN, a reduced elastic modulus $E^* = 50$ GPa, and a tip radius $R = 20$ nm; as the sensing depth of CR-AFM is about three times the contact radius, the substrate influence to our measurements is negligible for all the NWs tested.
[24] G. Wang and X. Li, Appl. Phys. Lett. **91**, 231912 (2007).